Smart Structures and Systems, *Vol. 15, No. 1 (2015) 15-40*
DOI: http://dx.doi.org/10.12989/sss.2015.15.1.015

Structural damage identification with power spectral density transmissibility: numerical and experimental studies

Jun Li[*1], Hong Hao[1a] and Juin Voon Lo[2b]

[1]Department of Civil Engineering, Curtin University, Kent Street, Bentley, WA 6102, Australia
[2]School of Civil and Resource Engineering, The University of Western Australia, 35 Stirling Highway, Crawley, WA 6009, Australia

(Received February 5, 2014, Revised April 30, 2014, Accepted May 5, 2014)

Abstract. This paper proposes a structural damage identification approach based on the power spectral density transmissibility (PSDT), which is developed to formulate the relationship between two sets of auto-spectral density functions of output responses. The accuracy of response reconstruction with PSDT is investigated and the damage identification in structures is conducted with measured acceleration responses from the damaged state. Numerical studies on a seven-storey plane frame structure are conducted to investigate the performance of the proposed damage identification approach. The initial finite element model of the structure and measured acceleration measurements from the damaged structure are used for the identification with a dynamic response sensitivity-based model updating method. The simulated damages can be identified accurately without and with a 5% noise effect included in the simulated responses. Experimental studies on a steel plane frame structure in the laboratory are performed to further verify the accuracy of response reconstruction with PSDT and validate the proposed damage identification approach. The locations of the introduced damage are detected accurately and the stiffness reductions in the damaged elements are identified close to the true values. The identification results demonstrated the accuracy of response reconstruction as well as the correctness and efficiency of the proposed damage identification approach.

Keywords: damage identification; response reconstruction; power spectral density transmissibility; frequency domain; model updating

1. Introduction

Vibration responses, i.e., accelerations, measured from structures are widely used for structural condition assessment with damage identification algorithms. The identification results can support structural health monitoring, service life prediction and reliability updating of structures. Numerous studies are conducted to perform the structural damage assessment by using modal information, e.g. frequencies, mode shapes, flexibility, frequency response function, and mode shape curvature, etc. Yan *et al*. (2007) summarized the recent development in the vibration-based

*Corresponding author, Lecturer, E-mail: junli@curtin.edu.au
[a] Professor, E-mail: hong.hao@curtin.edu.au
[b] Graduate student

http://www.techno-press.org/?journal=sss&subpage=8 ISSN: 1738-1584 (Print), 1738-1991 (Online)

structural damage detection techniques. Features of traditional damage detection methods based on those vibration properties listed above and modern methods based on wavelet analysis (Li *et al*. 2009), neural network and genetic algorithms are discussed.

Many available system identification techniques require both the measured input excitation and output responses. However, it is difficult to accurately measure the input excitations under operation conditions, such as winds, thermo and traffic loads. Therefore the desirable damage identification approaches are to estimate structure parameters only based on measured responses without measuring the input excitations. Wang and Haldar (1997) proposed an iterative least-squares procedure for system identification with unknown input excitation based on the extended Kalman filter method. Yang *et al*. (2007) performed least-squares estimation with unknown excitations for damage identification of structures. Perry and Koh (2008) proposed an output only structural identification strategy to identify the unknown stiffness and damping parameters. Yi *et al*. (2013) presented a multi-stage structural damage diagnosis method based on "energy-damage" theory. Studies on the simultaneous identification of structural parameters and input excitations have also been explored (Law and Li 2010, Huang *et al*. 2010, Lu *et al*. 2011, Xu *et al*. 2012, Lei *et al*. 2012, Lei *et al*. 2013). The computational effort of such methods may be significantly intensive due to a large number of unknown parameters, and the accuracy of damage identification results is dependent on the identified forces.

Transmissibility, which defines the output-to-output relationship, is receiving increased attention due to the independence on input excitations and its high sensitivity to local structural changes. Recently, the transmissibility in the frequency domain has been used for structural response reconstruction (Law *et al*. 2011) and damage identification of a substructure (Li *et al*. 2012). Yan and Ren (2012) proposed an operational modal identification approach based on the power spectrum density transmissibility from measured accelerations to a reference measurement for extracting frequencies and mode shapes of structures.

In this paper, the relationship between two sets of auto-spectral density functions of output responses is formulated and no reference point is required. This relationship is explored for structural response reconstruction, and a damage identification approach based on the power spectral density transmissibility (PSDT) is developed without measuring the input excitations. The damage identification is performed with a limited number of measured accelerations from structures. The accuracy of response reconstruction with PSDT is also investigated and the reliability and effectiveness of the proposed damage identification approach are validated. Numerical and experimental studies on a seven-storey plane frame structure are conducted to demonstrate the performance of the proposed response reconstruction and damage identification approach.

2. Response reconstruction with PSDT

The response reconstruction in a structure has been developed with the transmissibility in the frequency domain (Law *et al*. 2011). This paper further develops the response reconstruction by using auto-spectral density functions of two sets of output responses without the reference measurement. The power spectral density denotes the vibration energy of signals in the frequency domain and could increase the sensitivity to identify local damage. The formulation of PSDT will be developed, and structural damage identification is conducted from the measured acceleration responses based on the response reconstruction with PSDT and structural model updating.

2.1 Frequency response function

The general equation of motion of a damped structure with n Degrees-of-Freedom (DOFs) can be written as

$$[M]\{\ddot{x}(t)\}+[C]\{\dot{x}(t)\}+[K]\{x(t)\}=\{F(t)\} \tag{1}$$

where $[M]$, $[C]$ and $[K]$ are the $n\times n$ mass, damping and stiffness matrices of the structure respectively; $\{\ddot{x}(t)\}$, $\{\dot{x}(t)\}$ and $\{x(t)\}$ are respectively the nodal acceleration, velocity and displacement vectors of the structure; $\{F(t)\}$ is a vector of applied forces at the associated DOFs of the structure. Rayleigh damping $[C]=a_1[M]+a_2[K]$ is assumed in this study, where a_1 and a_2 are the Rayleigh damping coefficients.

The Fourier transform of Eq. (1) gives

$$\left(-\omega^2[M]+j\omega[C]+[K]\right)\{X(\omega)\}=\{F(\omega)\} \tag{2}$$

Therefore, the displacement response in the frequency domain is given as

$$\{X(\omega)\}=[H_d(\omega)]\{F(\omega)\}=\left(-\omega^2[M]+j\omega[C]+[K]\right)^{-1}\{F(\omega)\} \tag{3}$$

in which, $[H_d(\omega)]=\left(-\omega^2[M]+j\omega[C]+[K]\right)^{-1}$ is the displacement frequency response function (FRF) matrix. The FRF matrix represents the inherent system frequency response characteristics and it can be measured experimentally, reconstructed from an experimental modal analysis, or obtained from finite element analysis of the structure.

The acceleration response in the frequency domain could be obtained from Eq. (2) as

$$\{\ddot{X}(\omega)\}=-\omega^2\{X(\omega)\}=[H_a(\omega)]\{F(\omega)\}=-\omega^2[H_d(\omega)]\{F(\omega)\} \tag{4}$$

where $[H_a(\omega)]=-\omega^2[H_d(\omega)]$ is the acceleration FRF matrix.

2.2 Formulation of PSDT in the frequency domain

Assuming that there are two sets of responses: the First-set and the Second-set, which are also considered as the Known-set and Unknown-set response vectors $\ddot{X}_k(\omega)$ and $\ddot{X}_u(\omega)$ respectively, the following equation will be obtained in terms of Eq. (4)

$$\begin{cases}\ddot{X}_k(\omega)=H_a^k(\omega)F(\omega)\\ \ddot{X}_u(\omega)=H_a^u(\omega)F(\omega)\end{cases} \tag{5}$$

where $H_a^k(\omega)$ and $H_a^u(\omega)$ are the FRFs of the Known-set and Unknown-set, respectively. The dimensions of $H_a^k(\omega)$ and $H_a^u(\omega)$ matrices are $(l \cdot nfft)\times(q \cdot nfft)$ and $(m \cdot nfft)\times(q \cdot nfft)$ respectively assuming l, m, q and $nfft$ are the numbers of responses in the Known-set and Unknown-set, the number of external forces and the number of frequency lines in Fourier spectrum, respectively.

Define $G_{FF}(\omega)$ as the auto-spectral density function of the input excitations on the structure, and $G_{\ddot{X}_k\ddot{X}_k}(\omega)$ and $G_{\ddot{X}_u\ddot{X}_u}(\omega)$ the auto-spectral density functions of output acceleration responses of Known- and Unknown-sets, respectively, the following equation can be obtained (Bendat and Piersol 1980)

$$\begin{cases} G_{\ddot{X}_k\ddot{X}_k}(\omega) = \left|H_a^k(\omega)\right|^2 G_{FF}(\omega) \\ G_{\ddot{X}_u\ddot{X}_u}(\omega) = \left|H_a^u(\omega)\right|^2 G_{FF}(\omega) \end{cases} \tag{6}$$

When two or more responses are involved in the response vector, they will be assembled in a vector with one sensor data followed by those from other sensors. The response reconstruction equation between two auto-spectral density functions can be derived as

$$G_{\ddot{X}_u\ddot{X}_ur}(\omega) = PSDT(\omega)G_{\ddot{X}_k\ddot{X}_k}(\omega) \tag{7}$$

in which $PSDT(\omega)$ is the PSDT from the auto-spectral density $G_{\ddot{X}_k\ddot{X}_k}(\omega)$ at the Known-set to predict the auto-spectral density $G_{\ddot{X}_u\ddot{X}_ur}(\omega)$ at the Unknown-set. $PSDT(\omega)$ can be expressed as

$$PSDT(\omega) = \left|H_a^u(\omega)\right|^2\left(\left|H_a^k(\omega)\right|^2\right)^+ \tag{8}$$

where '+' denotes the pseudo-inverse of a matrix. The number of measurements in the Known-set response vector should be at least equal or larger than the number of excitation forces on the structure so that the pseudo-inverse of matrix $\left(\left|H_a^k(\omega)\right|^2\right)^+$ may exist. For the possible cases if have when the pseudo-inverse does not exist, the Damped Singular Value Decomposition (CSVD) or Truncated Singular Value Decomposition (TSVD) can be employed by eliminating those very small singular values to calculate the pseudo-inverse. Eq. (7) can be used for the structural response reconstruction with the available measured Known-set response to predict the response at the Unknown-set. PSDT can be computed with the FRFs calculated from the finite element model of the structure with Eq. (8).

The auto-correlation of a response $R_p(\tau)$ can be obtained from the statistical definition as

$$R_p(\tau) = E\left\{\ddot{x}_p(t)\ddot{x}_p(t+\tau)\right\} \tag{9}$$

where $\ddot{x}_p(t)$ denotes the response at the p-th DOF, and $E\{\bullet\}$ indicates the expectation operator. Eq. (9) can further be written as

$$\begin{aligned} R_p(\tau) &= \lim_{T\to\infty}\frac{1}{T}\int_0^T \ddot{x}_p(t)\ddot{x}_p(t+\tau)dt \\ &= \lim\frac{1}{NN}\sum_{n=0}^{NN}\left(\ddot{x}_p(n\Delta t)\ddot{x}_p(n\Delta t+\tau)\right) \end{aligned} \tag{10}$$

where NN is the number of data point within the duration T under studied.

2.3 First-Order-Hold input force approximation

In the structural dynamic response analysis, methods of discretising the continuous dynamic system model are applied. The model was discretised with the Zero-Order-Hold (ZOH) and First-Order-Hold (FOH) input discrete approximations, respectively. The ZOH discrete method generates a continuous input signal by holding each sample value constant over a sample interval, which is a normal discrete approach used in structural analysis. Whereas the FOH method uses linear interpolation between each sample interval to generate a continuous input sample as shown in Fig. 1. Previous studies have proven that FOH input force approximation can enhance the accuracy of the dynamic response analysis results compared with ZOH input force approximation (Darby *et al*. 2001) due to the smoothed input approximation generated for dynamic analysis.

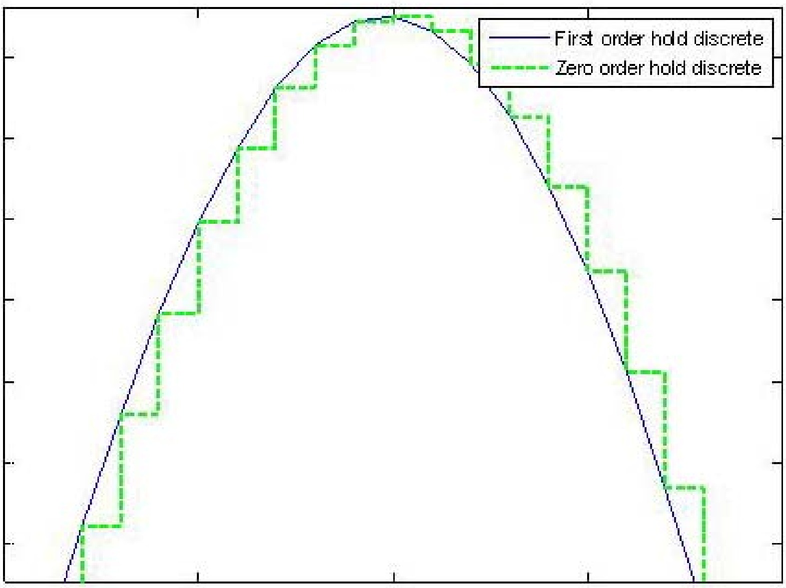

Fig. 1 ZOH and FOH input force approximations

2.4 Computational procedure for response reconstruction

If the initial finite element model of the structure in the undamaged state can be created, the information of time-histories of the applied force is not required in the response reconstruction process, but the locations of the applied forces should be known. Following describes the steps for response reconstruction:

Step 1: The dynamic acceleration response $\ddot{x}(t)$ of the structure is computed from Eq. (1) using numerical integration methods. The analytical Known-set and Unknown-set response vectors of the structure are obtained as the "measured" responses.

Step 2: These two sets of responses are transformed from the time domain into the frequency domain and then the auto-spectral density functions of responses are calculated as $G_{\ddot{X}_k\ddot{X}_k}(\omega)$ and $G_{\ddot{X}_u\ddot{X}_u}(\omega)$.

Step 3: FRF matrices $H_a^k(\omega)$ and $H_a^u(\omega)$ in Eq. (5) corresponding to the Known-set and Unknown-set at measurement DOFs are obtained from the finite element model of the structure.

Step 4: The obtained $H_a^k(\omega)$ and $H_a^u(\omega)$ matrices are then used to calculate the PSDT in Eq. (8) and the response reconstruction is performed with Eq. (7).

Step 5: Compare the reconstructed power spectral density $G_{\ddot{X}_u\ddot{X}_u r}(\omega)$ with the analytical one $G_{\ddot{X}_u\ddot{X}_u}(\omega)$. The relative error will be obtained by comparing these two spectra as

$$\text{Relative error} = \frac{\left\| G_{\ddot{X}_u\ddot{X}_u r}(\omega) - G_{\ddot{X}_u\ddot{X}_u}(\omega) \right\|_2}{\left\| G_{\ddot{X}_u\ddot{X}_u}(\omega) \right\|_2} \tag{11}$$

3. Structural damage detection

The parametric model updating method for damage identification is popular as they keep the connectivity and physical meaning of structures (Brownjohn *et al*. 2001). In this study, a dynamic response sensitivity-based finite element model updating method is used for the identification. The damage is assumed to be only related to a stiffness reduction such as a change in the elastic modulus. The mass matrix is assumed to be unchanged before and after the damage. The elemental stiffness factors in the initial intact structural finite element model are iteratively updated to have the reconstructed responses matching those measurements from the damaged state.

3.1 Damage model

Linear structural damage is assumed in this study, which means the initially linear structure is assumed to remain linear after the damage. The damaged system stiffness matrix K_d of the structure can be denoted as

$$[K_d] = \sum_{i=1}^{n} \alpha_i [K_i] = \sum_{i=1}^{n} (1 - \Delta\alpha_i)[K_i] \tag{12}$$

where $[K_i]$ and α_i are the i th elemental stiffness matrix of the undamaged structure and the i th elemental stiffness factor in the damage state, respectively. $\Delta\alpha_i$ represents the stiffness reduction of the i th element, and it is a positive value.

3.2 Damage identification algorithm

The objective function of the damage identification algorithm is defined as the difference between two sets of auto-spectral density functions

$$f_{obj} = \left\| G_{\ddot{X}_u \ddot{X}_u r}(\omega) - G_{\ddot{X}_u \ddot{X}_u}(\omega) \right\|_2 \tag{13}$$

where $G_{\ddot{X}_u \ddot{X}_u}(\omega)$ is the calculated auto-spectral power density of the measured Second-set response vector from the damaged structure. $G_{\ddot{X}_u \ddot{X}_u r}(\omega)$ is the reconstructed auto-spectral power density of the Second-set response vector from Eq. (7) with the measured First-set response vector $G_{\ddot{X}_k \ddot{X}_k}(\omega)$. Structural elemental stiffness factors are then iteratively updated by minimizing the objective function in Eq. (13) to make these two auto-spectral density functions as close as possible.

The dynamic response sensitivity-based model updating method (Lu and Law 2007) has been used to perform the damage identification and it is adopted here to identify the damage in the structure

$$[S]\{\Delta\alpha\} = \{\Delta\ddot{x}\} = \{\ddot{x}_{2m}\} - \{\ddot{x}_{2r}\} \tag{14}$$

where, $\{\Delta\alpha\}$ is the perturbation of the vector of structural elemental stiffness factors, $[S]$ is the sensitivity matrix of $G_{\ddot{X}_u \ddot{X}_u r}(\omega)$ with respect to the elemental stiffness factors. The objective function in Eq. (13) is an implicit function with respect to the elemental stiffness factors. The sensitivity matrix $[S]$ is obtained using numerical finite difference method (Zivanovic *et al*. 2007, Morton and Mayers 2005). It is noted that the number of equations in Eq. (14) should be larger than the number of unknown elemental stiffness parameters to make sure that the identification is over-determined. The adaptive Tikhonov regularization method (Li and Law 2010) is used to obtain the solution of Eq. (14) to improve identification results with noisy measurements. The L-curve method (Hansen 1992) is used to obtain the regularization parameter.

3.3 Sensitivity matrix computation

The sensitivity matrix is a rectangular matrix of order $q \times U$, where q and U are the number of target responses in Eq. (13) and system parameters to be identified, respectively

$$[S] = [S_1, S_2, \cdots, S_U] = \left[\frac{\partial G_{\ddot{X}_u \ddot{X}_u r}(\omega)}{\partial P_{j=1,2,\cdots,U}} \right] \tag{15}$$

$S_j \ (j = 1, 2, \cdots, U)$ is the sensitivity of the target auto-spectral density function to a certain change in parameter P_j. Elements of the sensitivity matrix can be calculated numerically using, for example, the forward finite difference approach

$$S_j = \frac{G_{\ddot{X}_u \ddot{X}_u r}(P_j + \Delta P_j) - G_{\ddot{X}_u \ddot{X}_u r}(P_j)}{\Delta P_j} \tag{16}$$

where $G_{\ddot{X}_u \ddot{X}_u r}(P_j)$ is the reconstructed power spectral density at the current state of the parameter P_j, while $G_{\ddot{X}_u \ddot{X}_u r}(P_j + \Delta P_j)$ is the reconstructed power spectral density when the parameter P_j is increased by an increment ΔP_j. The selection of ΔP_j may have a effect on the identification accuracy, however, based on authors' experiences with many trails with different values of increments, the identification results are converged if a relatively small increment is used such as 0.001 or 0.0001.

3.4 Iterative damage identification procedure

Acceleration measurements from the structure in the damaged state will be used to identify the elemental stiffness factors iteratively. Initially the elemental stiffness factor of every element in the finite element model is set as unity. An updated finite element model is assumed to be available as a reference model for the following iterative procedure of damage identification.

Step 1: Measure the dynamic acceleration responses $\{\ddot{x}_k(t)\}$ and $\{\ddot{x}_u(t)\}$ from the damaged structure and transform them into the frequency domain to calculate the auto-spectral density functions $G_{\ddot{X}_k \ddot{X}_k}(\omega)$ and $G_{\ddot{X}_u \ddot{X}_u}(\omega)$ with Eq. (10), respectively.

Step 2: Compute the FRF matrices $H_a^k(\omega)$ and $H_a^u(\omega)$ from the finite element model of the initial structure. PSDT is then calculated with Eq. (8).

Step 3: Perform the response reconstruction with Eq. (7) and calculate the difference vector between the auto-spectral density function $G_{\ddot{X}_u \ddot{X}_u}(\omega)$ in Step 1 and the reconstructed one $G_{\ddot{X}_u \ddot{X}_u r}(\omega)$. The sensitivity matrix $[S]$ of $G_{\ddot{X}_u \ddot{X}_u r}(\omega)$ with respect to structural elemental stiffness factors is obtained by using the numerical finite difference method.

Step 4: Obtain the perturbation vector of elemental stiffness factors $\{\Delta\alpha\}$ from Eq. (14) with the adaptive Tikhonov regularization technique.

Step 5: The vector of structural elemental stiffness factors is iteratively updated with $\alpha_{i+1} = \alpha_i + \Delta\alpha$ for the next iteration. Repeat Steps 2 to 4 until the following convergence criterion is satisfied

$$\frac{\left\|\alpha_{i+1}-\alpha_i\right\|_2}{\left\|\alpha_i\right\|_2} \leq Tolerance \tag{17}$$

where i denotes the ith iteration. The *tolerance* value is taken as 1.0×10^{-4} in the numerical study and 1.0×10^{-3} in experimental study.

It should be noted that the finite element model updating could be performed by directly matching the analytical power spectral density function with the measured ones to identify the damage in structures. However, this requires information of the input excitation in the finite element analysis to obtain the analytical power spectral density functions. In real situations, the input excitations are often not easy to be measured. One main and significant advantage of the proposed damage identification approach is that the excitation is not required in the identification process, and therefore only the structural parameters are formulated in the iterative identification procedure.

4. Numerical studies

Numerical studies on a seven-storey plane frame structure are conducted to demonstrate the accuracy of the proposed approach for structural response reconstruction and damage identification with PSDT. Fig. 2 shows the finite element model of the frame structure. The cross-sectional area and moment of inertia of the frame element are 0.32 m^2 and 0.017 m^4 respectively. The finite element model consists of 49 planar frame elements and 44 nodes with 3 DOFs for each node. Nodes 1 and 44 are fixed supports. Hence, the model has a total of 126 DOFs. The Young's modulus and mass density of material are respectively $3.5\times10^4 MPa$ and 2500 kg/m^3. The first seven natural frequencies of the structure are 2.43, 7.82, 14.72, 22.56, 23.94, 31.42 and 33.93 Hz, respectively. Rayleigh damping is assumed and the damping ratios for the first two modes are defined as $\xi = 0.012$. Two forces F1 and F2 with multiple sine excitations are applied on the structure as shown in Fig. 2. These two forces are

$$F1=\begin{cases}200\left(\sin\left(30\pi t\right)+0.5\sin\left(15\pi t\right)+0.2\sin\left(60\pi t\right)\right), & t\leq 1s\\ 0, & t>1s\end{cases} \quad \text{and}$$

$$F2=\begin{cases}200\left(\sin\left(50\pi t\right)+0.6\sin\left(75\pi t\right)+0.2\sin\left(100\pi t\right)\right), & t\leq 1s\\ 0, & t>1s\end{cases}$$

In order to obtain the frequency domain analysis results under the excitation forces accurately, the following parameters are defined as shown in Fig. 3: the duration of the excitation force t_d, the duration of free vibration t_f and the total sampling time T_0. Since the peak response of the system may be obtained after the excitation has ended, the analysis is carried out over a time duration T_0 which is much longer than t_d. Furthermore, it has been reported (Chopra 2007) that the classical discrete Fourier transform solution will become increasingly accurate as the duration t_f of free vibration becomes longer because T_0 should be long enough for the free vibration of the system to damp out to small motion at the end of the period T_0. On the other hand, in order to obtain the frequency domain responses accurately, the sampling interval Δt should be short enough compared both to the periods of significant harmonics in the excitation and to the natural period of the structure.

Therefore in this study the duration t_d of the above excitation forces is limited to the first one second and the duration of measurement is taken as 16.384s to ensure that T_0 is long enough for the system responses to decay to zero and the number of sampling points is a power of two for the Fourier transform. The sampling rate is set at 1000 Hz to ensure a good accuracy of discrete Fast Fourier Transform (FFT) for the frequency domain response analysis. Studies under seismic excitations (Li and Law 2012) and moving load excitations (Li *et al*. 2013) are explored in previous works, however, it should be noted that multi-sine excitation is used in this simulation study to reduce the leakage effects and to produce responses that are of better quality as compared with the random noise excitation, especially when only short time sequences can be recorded from the structure (Verboven *et al*. 2004).

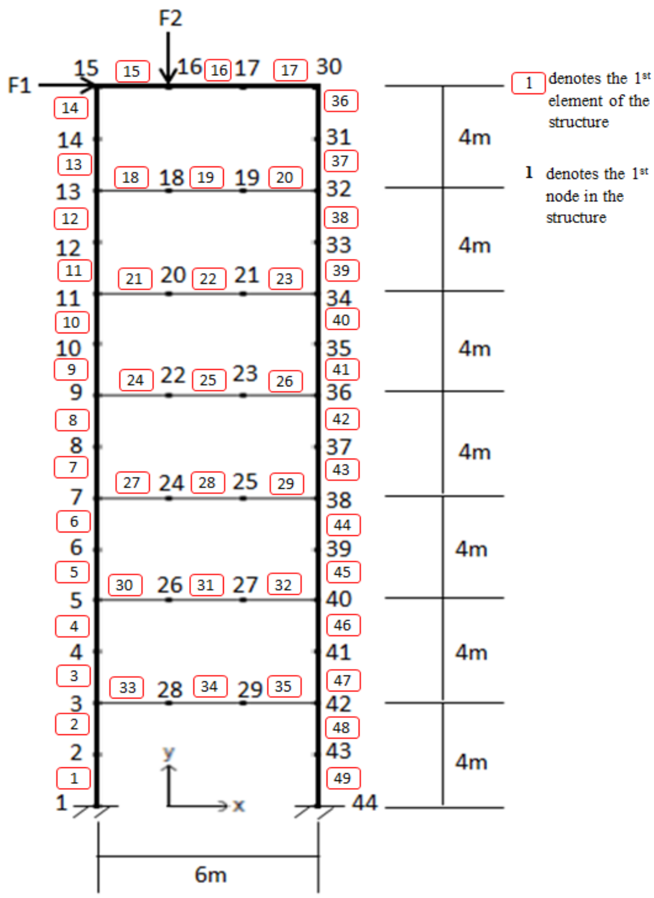

Fig. 2 Finite element model of the frame structure in numerical study

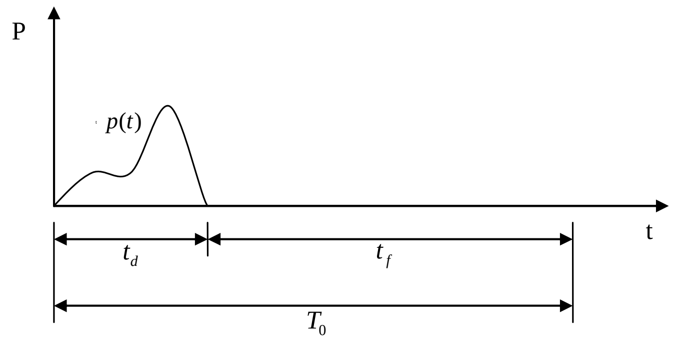

Fig. 3 A schematic excitation force and sampling duration

4.1 Structural response reconstruction

Dynamic analysis of the frame model is performed, and response reconstruction with PSDT is conducted to investigate the accuracy of the proposed approach. Six sensors are placed arbitrarily on this structure and their locations are Node 11(x), 13(y), 15(x), 30(y), 32(x) and 35(y) where "11(x)" denotes that the sensor is placed along the *x* direction at Node 11. The response calculation is conducted using ZOH and FOH input force approximations, respectively. The responses from these six sensor locations are simulated (measured) and they are taken as the Known-set response vector. The responses from the remaining DOFs are considered as the Unknown-set which will be reconstructed with Eq. (7). The relative error is calculated between the analytical and reconstructed power spectral density functions.

Fig. 4 shows the relative errors of the response reconstruction results at all the remaining DOFs. The response reconstruction errors from FOH responses are generally less than those from ZOH responses indicating that accurate input approximate for dynamic analysis can provide more accurate response analysis results with a closer discrete form of input forces. The maximum errors under ZOH and FOH force approximations are observed both at the 60th DOF and their errors are 6.66% and 1.45%, respectively. Figs. 5(a) and 5(b) show the true and reconstructed responses at the 60th DOF with ZOH and FOH approximations, respectively. It is demonstrated that the response reconstruction with PSDT can achieve a good accuracy, and the reconstruction with FOH has a better accuracy than with ZOH.

4.1.1 Effect of sampling duration and sampling rate

The sampling duration and sampling rate have been considered as two significant factors that could influence the accuracy of frequency domain analysis and the subsequent response reconstruction. In order to study how these two factors affect the response reconstruction accuracy, the sampling duration is considered varying from 4.192s to 32.768s and the sampling rate varies from 250 Hz to 2000 Hz in this study. When the sampling time varies, the sampling rate is kept constant at 1000 Hz. When the sampling rate varies, the sampling time is set equal to 16.384s. Table 1 lists the average relative errors of the response reconstruction results in the auto-spectral density functions with different sampling duration and sampling rate settings. Note that the average error denotes the mean values of relative errors from all the DOFs in the Unknown-set. It may be concluded from Table 1 that when a longer sampling time or a higher sampling rate is used, more accurate response reconstruction results can be obtained since more number of sampling points are recorded for FFT.

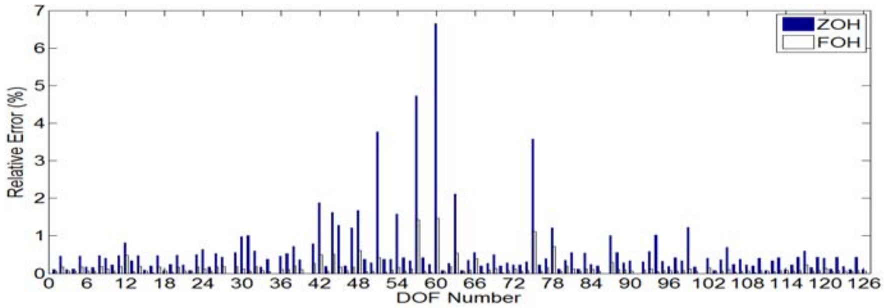

Fig. 4 Relative errors of response reconstruction results

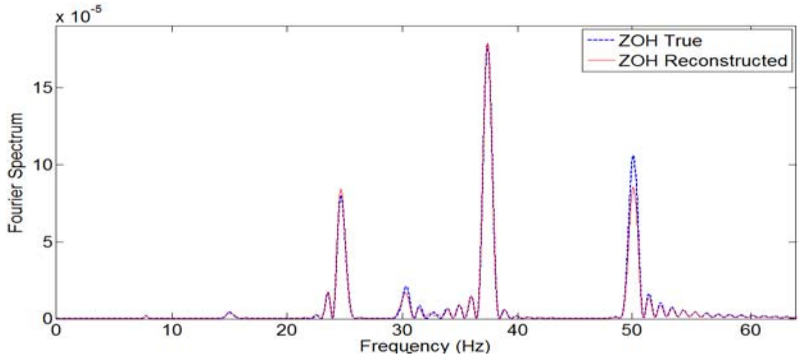

(a)

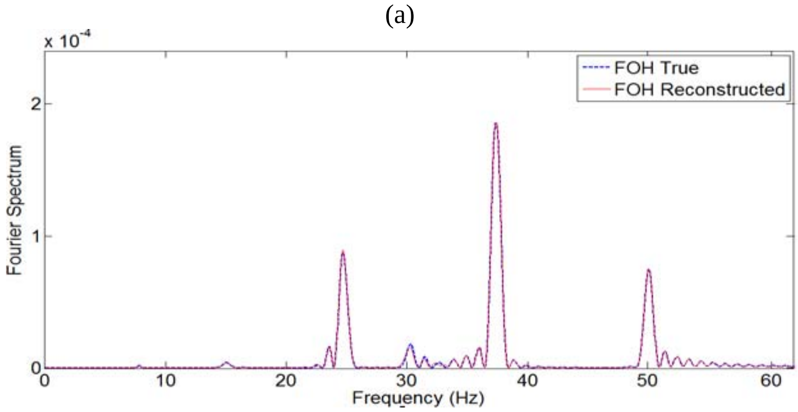

(b)

Fig. 5 Analytical and reconstructed responses at the 60^{th} DOF. (a) ZOH input force approximation; (b) FOH input force approximation

Table 1 Errors (%) in the response reconstruction with different sampling duration and rate

Sampling Time (s) (Sampling rate=1kHz)		4.096	8.192	16.384	32.768
Average error (%)	ZOH	0.62	0.56	0.55	0.55
	FOH	0.22	0.15	0.14	0.14
Sampling Rate (Hz) (Sampling time = 16.384s)		250	500	1000	2000
Average error (%)	ZOH	11.9	2.30	0.55	0.20
	FOH	0.84	0.25	0.14	0.13

4.1.2 Effect of noise in measured responses

To simulate the effect of measurement noise, a normally distributed random noise with zero mean and unit standard deviation is added to the calculated dynamic response as,

$$\ddot{x}_n = \ddot{x}_{cal} + E_p N_{oise} std(\ddot{x}_{cal}) \tag{18}$$

where $\ddot{x}_n$ and $\ddot{x}_{cal}$ are simulated noisy response and original calculated response, respectively; E_p is the noise level; N_{oise} is a standard normal distribution vector with zero mean and unit standard deviation and $std(\ddot{x}_{cal})$ denotes the standard deviation of the original calculated response. E_p equals to 0.1 when the noise level is 10%.

The response analysis under ZOH and FOH approximations is performed respectively and 10% noise effect is added in the measurements. Fig. 6 shows the simulated acceleration responses at sensor location Node 15(x) under FOH without noise and with 10% noise. Designed filters and wavelet techniques can be used to reduce the noise effect and smooth signals (Yi *et al*. 2012). Since the first seven natural frequencies of the structure are lower than 50 Hz and therefore the “polluted” measured responses are then filtered using a low-pass filter with a cutoff frequency of 100 Hz which is much higher than the frequency of interest in this study. These filtered data are then used for response reconstruction. Table 2 shows the relative errors in the response reconstruction results with different sampling duration and sampling rates and 10% noise effect. The comparison between Tables 1 and 2 shows that the noise effect would increase the reconstruction error, especially for the case with a lower sampling rate and shorter sampling duration. Table 2 also demonstrates that a higher sampling rate and longer sampling duration such as 1000 Hz and 16.384s for the example in this study lead to a good reconstruction under noise effect.

Table 2 Errors (%) in the response reconstruction with different sampling duration and rate under noise effect

Sampling Time (s) (Sampling rate=1kHz)		4.096	8.192	16.384	32.768
Average error (%)	ZOH	1.51	1.51	0.18	0.56
	FOH	1.25	1.17	0.88	0.15
Sampling Rate (Hz) (Sampling time = 16.384s)		250	500	1000	2000
Average error (%)	ZOH	22.7	4.69	1.69	1.38
	FOH	4.31	2.43	1.67	1.20

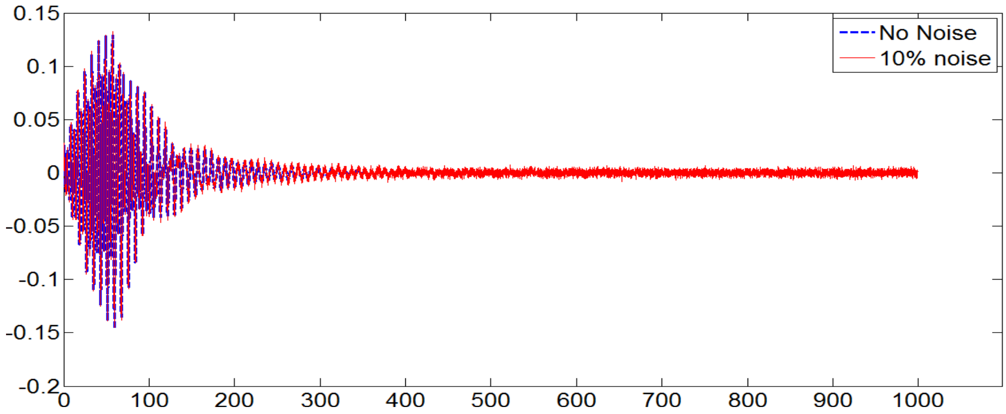

Fig. 6 Accelerations at Node 15(x) under FOH without and with noise

4.2 Structural damage identification

The response reconstruction accuracy with PSDT has been verified in the above sections. Several parameters that are considered potentially to affect the accuracy of the reconstruction process have been investigated. It has been demonstrated that response reconstruction under FOH discrete has a better accuracy than that under ZOH, and therefore the damage identification will be conducted by using response calculated from FOH approximations to simulate a realistic input to the structures. In this study damage is introduced into the structure as a reduction of elastic modulus in a specific element. 10% damage is introduced into the 3rd and the 10th element of the structure as an example. Eight sensors are placed on the structure and they are divided into two sets, as shown in Table 3. Acceleration responses in these two sets from the damaged structure are measured and transformed into the frequency domain to calculate the auto-spectral density functions. The sampling duration and sampling rate of the used data are 16.384s and 1000 Hz, respectively. With the available finite element model of the initial intact structure, the FRF matrix can be computed and used to obtain the PSDT. The response difference between the measured and reconstructed Second-set auto-spectral density functions is obtained. The sensitivity-based finite element model updating is then used to conduct the damage identification with an iterative procedure described above in Section 3.4. The identification is performed with measured responses without and with 5% noise, respectively.

Fig. 7 shows the damage identification results for the cases without and with noise effect in the measured responses. For the noise-free case, the identified damage extents in the 3rd and 10th elements are 9% and 10.37%, respectively. For the case with 5% noise, the identified damages are 8.07% and 11.85% respectively at the two elements. The identified results from both cases are close to the true introduced damage values at the correct damage locations. It should be noted that several false identifications exist in the results for the case with noise, especially in the elements which are adjacent to the true damaged elements, e.g., 2nd and 4th elements, due to the smearing effect. Nonetheless, the identification results demonstrate that the introduced damages are identified effectively with a close damage level estimation to the true values.

Table 3 Sensor locations for damage identification

Sensor set	Sensor locations
First-set (Known-set)	Node 3(x), 5(x), 7(x), 9(x), 11(x), 13(x)
Second-set (Unknown-set)	8(x), 14(x)

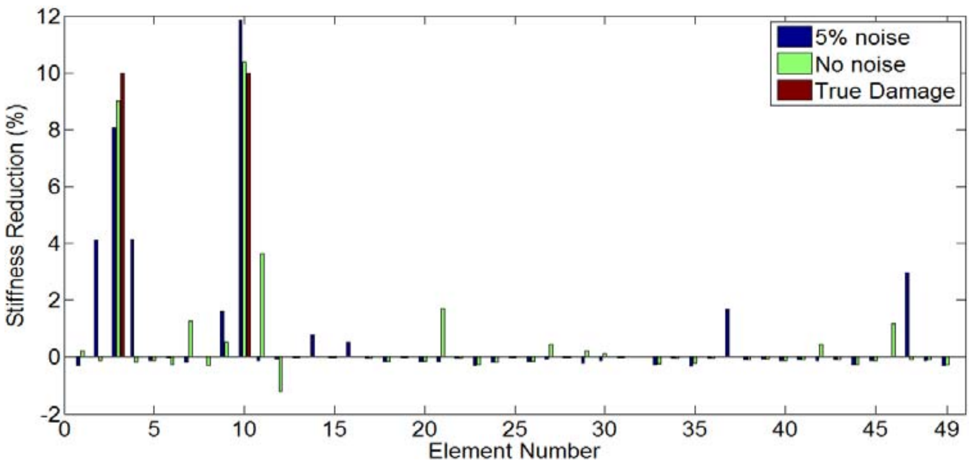

Fig. 7 Damage identification results without and with noise effect

5. Experimental verification

5.1 Experimental setup

Experimental studies on a seven-storey steel plane frame are conducted to validate the reliability and effectiveness of the proposed approach. Measured acceleration responses with measurement and environmental noise are used for the structural response reconstruction and damage identification. The dimensions of the frame are shown in Fig. 8. The column of the frame has a total height of 2.1 m with 0.3 m for each storey. The length of the beam is 0.5 m. The cross-sections of the column and beam elements are measured as 49.98 mm × 4.85 mm and 49.89 mm × 8.92 mm, respectively. The mass densities of the column and beam elements are measured as 7850 kg/m^3 and 7734.2 kg/m^3, respectively. Fig. 9 shows the constructed steel frame building in the laboratory. The initial Young's modulus of the steel frame is taken as 210GPa for all elements. The connections between column and beam elements are continuously welded at the top and bottom of the beam section. Two pairs of mass blocks with approximately 4 kg weight each, are fixed at the quarter and three-quarter length of the beam in each storey to simulate the mass from the floor of a building structure. The bottoms of two columns of the frame are welded onto a thick and solid steel plate which is fixed to the ground as the boundary conditions of the frame. B&K3023 and KD1010 accelerometers and B&K signal conditioner are employed to measure the accelerations of the frame structure in dynamic tests. A SINOCERA LC-04A hammer is used to apply an impact excitation to the frame. A National Instruments data acquisition box is used to communicate with sensors and record the signals. The data recording computer and data acquisition board are electrically grounded to reduce the disturbance of AC power effect on the measured signals.

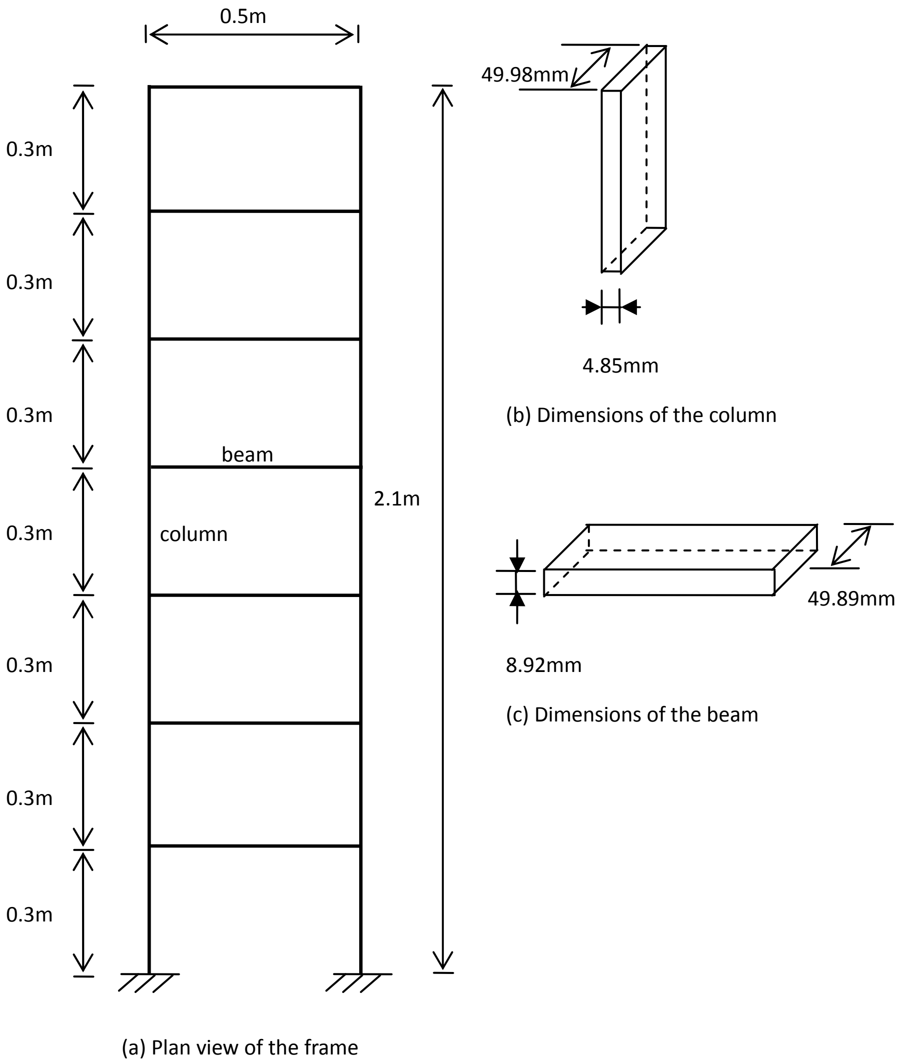

Fig. 8 Dimensions of the steel frame structure

Fig. 9 The laboratory steel frame model

5.2 Finite element model updating

An initial finite element model is built with planar elements to match the experimental model. Fig. 10 shows the finite element model of the frame structure, which includes 65 nodes and 70 planar frame elements. The weights of steel blocks are added at the corresponding nodes of the finite element model as concentrated masses. Each node has three DOFs (two translational displacements x, y and a rotational displacement θ), and the system has 195 DOFs in total. The translational and rotational restraints at the supports, which are Nodes 1 and 65, are represented initially by a large stiffness of 3×10^9 N/m and 3×10^9 N·m/rad, respectively.

Experimental modal analysis is performed to extract the natural frequencies and mode shapes of the frame structure from the measured acceleration responses by using peak-picking method and frequency domain decomposition method. Eight sensors were deployed in the hammer tests with one defined as the reference sensor and the others as moving sensors and placed at all the joints between the columns and beams. Repeated tests with the moving sensors placed at all beam-column joints were conducted. The first seven modes are significant as this is a seven-storey frame similar to a shear-type building, and higher modes are local modes. Fig. 11 shows the natural frequencies and mode shapes of the first seven modes. Rayleigh damping is assumed in this study. The first two damping ratios of the intact frame structure are obtained from the half-power bandwidth method as 0.0017 and 0.0012, respectively.

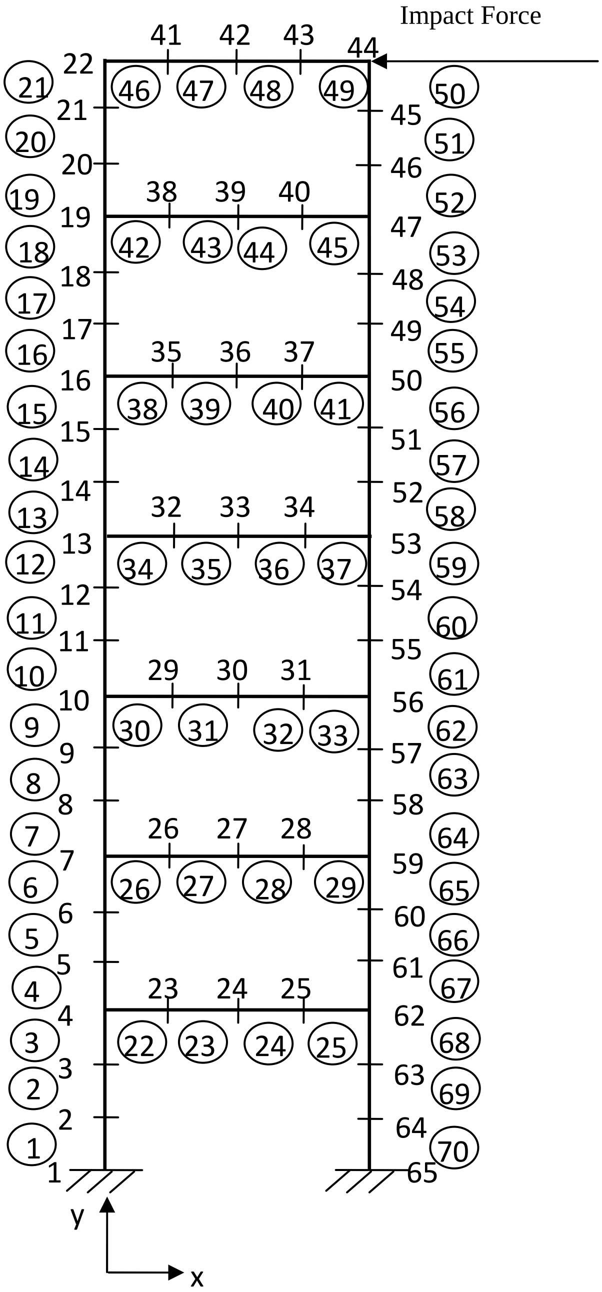

Note: (1): 1 denotes the node number
(2): 1 denotes the element number in the structure

Fig. 10 Finite element model of the planar frame structure

Model updating is required to match the analytical finite element model to the experimental frame model for investigating the accuracy of the proposed response reconstruction and damage identification approach with PSDT. The discrepancies between the experimental model and the created analytical finite element model are minimized by performing a two-stage model updating scheme. In the first-stage of model updating, the elastic modulus of each element and stiffness of restraints are selected as updating parameters. Modal information, such as measured frequencies and mode shapes are used for updating with the first-order modal sensitivity method (Friswell and Mottershead 1995). Based on the updated results obtained above, the second-stage model updating further refines the updated model by using the dynamic response sensitivity method (Lu and Law 2007), which is targeted to have the dynamic responses calculated from the finite element model matching those measured ones as closely as possible. The elastic modulus of all the elements of the frame is selected in the second-round updating. Finally, an accurate updated finite element model which matches the experimental model well in both the modal information and the vibration responses is obtained (Li *et al*. 2012). This updated finite element model is then used as the baseline model in this paper for the following studies of dynamic response reconstruction and damage identification.

5.3 Verification on structural response reconstruction

The accuracy of forward structural response reconstruction will be investigated with the measured responses from impact tests on the intact frame structure. The impact was applied at Node 44, which is the beam-column joint at the 7$^{\text{th}}$ floor of the right column as shown in Fig. 10. Eight sensors were employed to measure the responses of the frame structure. Measured responses from six sensor locations at Node 4(x), 10(x), 13(x), 19(x), 22(x) and 59(x) are taken as the First-set response to predict responses at other two sensor locations at Node 7(x) and 16(x) as the Second-set response. The baseline model is used to calculate the frequency response function and then PSDT with Eq. (8). The sampling rate is 1000 Hz and the sampled data within the first 16.384s are used to make sure the number of data points is a power of two. It may be noted that the reconstruction with Eq. (7) is conducted with measured acceleration responses only, and the hammer impact force is not required. Fig. 12 shows the measured and reconstructed responses at Node 16(x). The reconstructed response matches well with the measured one, which indicates the response reconstruction is accurate. The relative errors between the measured and reconstructed responses at Node 16(x) and 7(x) are 2.97% and 1.03%, respectively.

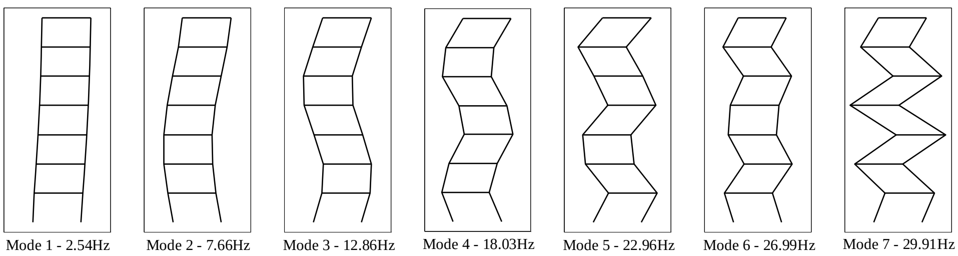

Fig. 11 Measured frequencies and mode shapes of the initial laboratory frame structure

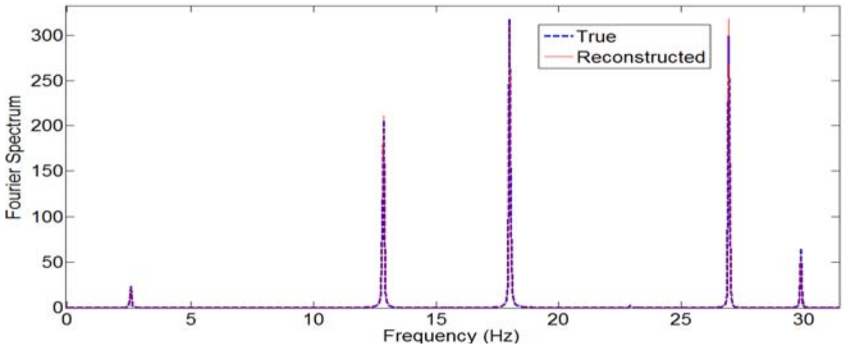

Fig. 12 Measured and reconstructed responses at Node 16(x)

Table 4 Errors (%) in the response reconstruction with different sampling durations and rates

Sampling Time (s) (Sampling rate=1kHz)		8.192	16.384	32.768
Sensor location	7(x) 16(x)	1.58 3.35	1.03 2.97	1.03 2.50
Sampling Rate (Hz) (Sampling time = 16.384s)		250	500	1000
Sensor location	7(x) 16(x)	1.04 2.97	1.03 2.97	1.03 2.97

In order to investigate the effect of the sampling duration on the response reconstruction accuracy, the sampling rate is kept as 1000 Hz while the sampling duration varies from 8.192s to 32.768s. Similarly to study the effect of the sampling rate, the sampling duration is set as a constant of 16.384s and the sampling rate is varied from 250 Hz to 2000 Hz. Table 4 lists the relative errors with different sampling duration and rates. Generally longer sampling duration gives more accurate response reconstruction accuracy. However, the accuracy of response reconstruction is not affected by the sampling rate. It can be seen from Table 4 that response reconstruction with sampling duration 32.684s and sampling rate 1000 Hz gives a better result and these settings will be used for the subsequent damage identification.

5.4 Damage identification

The length of each finite element in the frame structure is 100 mm. The damage was introduced as two cuts with width b = 30 mm and depth d = 10 mm, as shown in Fig. 13. A damage scenario with a single damage in element No. 12 is defined. Fig. 14 shows the damage scenario introduced in the frame structure. The equivalent stiffness reduction in the damaged element can be approximately obtained from the displacement method in the finite element analysis (Zhu and Xu 2005). The required force to produce a unit displacement at a specific DOF can be represented as the stiffness value. The analytical stiffness reduction in the damaged element is derived as 12.5% and considered as the true damage extent. Hammer impact excitation was applied at Node 44(x) of the frame structure, as shown in Fig. 10. Hammer impact tests were conducted in the damaged state and acceleration response data from the structure were recorded for damage identification.

The stiffness reduction in a specific element can be identified as the change in the elemental stiffness factors with respect to the baseline model.

In order to provide the spatial information and improve the robustness of the damage identification approach with experimental data, the first seven measured mode shapes are additionally included in the objective function as

$$f_{obj} = \left\| \left(G_{\ddot{X}_u \ddot{X}_u r}(\omega) - G_{\ddot{X}_u \ddot{X}_u}(\omega) \right), \left(Mode_m - Mode_a \right) \right\|_2 \tag{19}$$

where $Mode_m$ and $Mode_a$ are measured and analytical mode shape values of the frame, respectively. The same iterative damage identification procedure in Section 3.4 will be followed to identify the damage locations and extents.

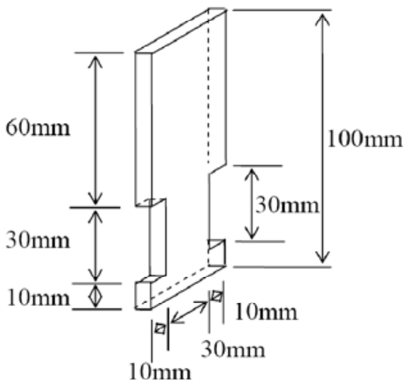

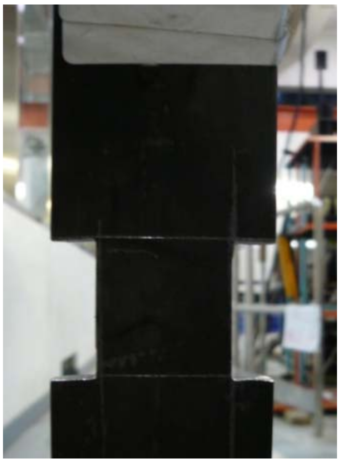

Fig. 13 Width and depth of the cut in the damaged element

Table 5 Identified frequencies of the frame structure

Frequency (Hz)	Undamaged	Damaged	Reduction (%)
Mode 1	2.54	2.526	0.55
Mode 2	7.66	7.658	0.03
Mode 3	12.86	12.816	0.34
Mode 4	18.03	18	0.17
Mode 5	22.96	22.842	0.51
Mode 6	26.99	26.974	0.06
Mode 7	29.91	29.73	0.6

Fig. 14 Introduced damage scenario in the frame structure

After the single damage is introduced, an impact test with sensors placed at beam-column joints Node 4(x), 7(x), 10(x), 13(x), 16(x), 19(x), 47(x), 50(x), 53(x) and 56(x) was performed to extract the frequencies and mode shapes. The obtained frequencies are listed in Table 5 and compared with those in the undamaged state. The maximum reduction in the frequency is 0.6% in the seventh mode. Such a small change in the frequency means a very minor damage is introduced into the frame, which is not easy to be confidently identified with traditional modal information based methods.

Another sensor placement is used, as shown in Table 6, and the measured responses from the damaged structure are used for the damage identification. The measurements are divided into two sets, in which the First-set response is used to predict the Second-set response with PSDT. The first two damping ratios are computed as 0.0019 and 0.0013 for the first two modes with the half-power bandwidth method. Rayleigh damping is assumed in this study and the experimental Rayleigh damping coefficients are computed with measured frequencies and damping ratios. The measured responses in both the First- and Second-set are low-pass filtered with a cutoff frequency of 36 Hz. Fig. 15 shows the calculated power spectral density function of the measured response at Node 7(x). The data points around the frequency peaks in the power spectrum and measured seven mode shapes are included in the objective function for the damage identification.

The iterative identification procedure is converged after 6 iterations. Fig. 16 shows the damage identification results without and with including measured mode shapes after 5 and 6 iterations, respectively. The identified damage extents in the introduced damaged 12th element are 17.76% and 13.36% without and with modal information, respectively. Identification including modal information gives improved results with a closer damage level estimation, which indicates that the damage can be identified effectively with the proposed approach.

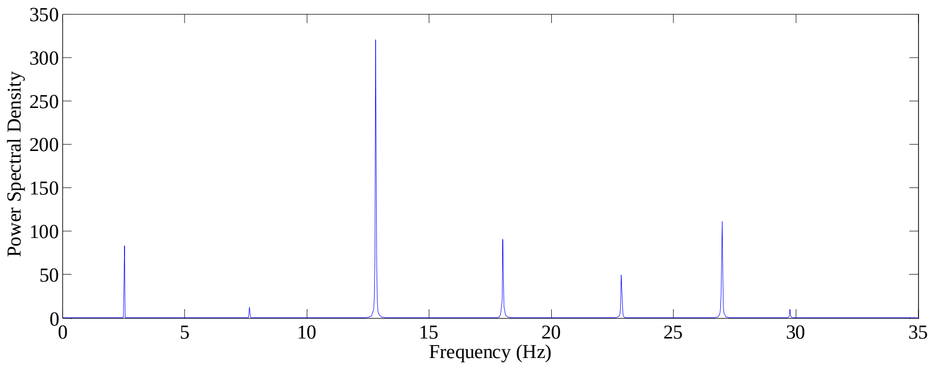

Fig. 15 Measured power spectral density at Node 7(x)

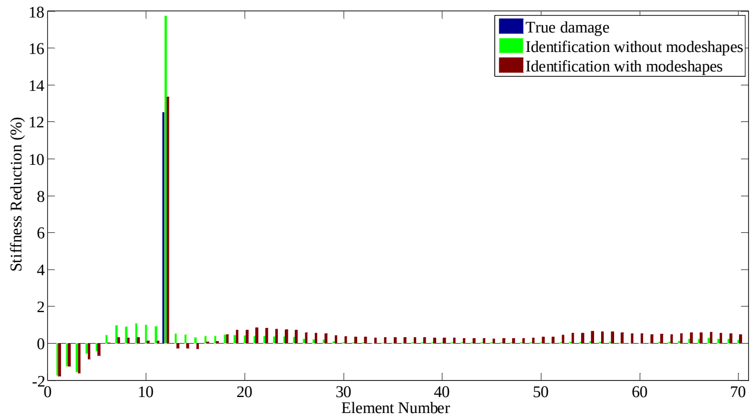

Fig. 16 Damage identification results in experimental study

Table6 Sensor placement configurations of Scenario A

Sensor Placement Configuration	Sensor Locations
First-set	Node 4(x), 7(x), 11(x), 15(x), 17(x), 47(x), 53(x)
Second-set	50(x), 56(x)

6. Conclusions

This paper proposes a structural damage identification approach without the information of the input excitations applied to the structure. The response reconstruction based on PSDT is performed in the frequency domain to reconstruct the auto-spectral density functions at locations without measured responses. The damage identification is conducted by minimizing the difference between the measured and the reconstructed power spectral density functions. The dynamic response sensitivity-based model updating method is used to formulate the damage identification algorithm. Measured acceleration responses from the damaged substructure and the initial finite element model of the intact frame are used for identification analysis.

Numerical and experimental studies on a seven-storey plane frame are conducted to investigate the performance of the damage identification approach. In numerical studies, the accuracy of the proposed response reconstruction technique is demonstrated and the effects of sampling duration, sampling rate and measurement noise are investigated. Two damages are introduced into the structure, and measured acceleration responses from the damaged structure without and with noise effect are used for damage identification. The damage locations and extents can be identified effectively for both the noise-free and noisy cases. Experimental studies on a steel frame model are conducted to validate the proposed response reconstruction and damage identification approach. Measured responses from hammer excitation are used for the initial finite element model updating, and the updated finite element model is taken as the baseline model for the damage identification. Measured responses from the intact frame are used to investigate the accuracy of response reconstruction with different sampling duration and rates. Good response reconstruction accuracy is achieved. Acceleration measurements from hammer tests on the damaged frame are used for the damage identification. The identification results demonstrate that the proposed damage identification approach can identify the location of the damage level accurately.

Acknowledgements

The work described in this paper was supported by Australian Research Council Discovery Early Career Researcher Award DE140101741, “Development of a Self-powered Wireless Sensor Network from Renewable Energy for Integrated Structural Health Monitoring and Diagnosis”.

References

Bendat, J.S. and Piersol, A.G. (1980), *Engineering Applications of Correlation and Spectral Analysis*, John Wiley & Sons, USA.

Brownjohn, J.M.W., Xia, P.Q., Hao, H. and Xia, Y. (2001), “Civil structure condition assessment by FE model updating: methodology and case studies”, *Finite. Elem. Anal. Des*, **37**(10), 761-775.

Chopra, A.K. (2007), *Dynamics of Structures: Theory and Applications to Earthquake Engineering*, Upper Saddle River, NJ: Prentice Hall, U.S.

Darby, A., Blakeborough, A. and Williams, M. (2001), “Improved control algorithm for real-time substructure testing”, *Earthq. Eng. Struct. D*, **30**(3), 431-448.

Friswell, M.I. and Mottershead, J.E. (1995), *Finite element model updating in structural dynamics*, Kluwer Academic Publishers, Dordrecht.

Hansen, P.C. (1992), “Analysis of discrete Ill-posed problems by means of the L-curve”, *SIAM Rev.*, **34**(4),

561-580.
Huang, H., Yang, J.N. and Zhou, L. (2010), "Adaptive quadratic sum-squares error with unknown inputs for damage identification of structures", *Struct. Control. Health.*, **17**(4), 404-426.
Law, S.S. and Li, J. (2010), "Updating the reliability of a concrete bridge structure based on condition assessment with uncertainties", *Eng. Struct*, **32**(1), 286-296.
Law, S.S., Li, J. and Ding, Y. (2011), "Structural response reconstruction with transmissibility concept in frequency domain", *Mech. Syst. Signal. Process*, **25**(3), 952-968.
Lei, Y., Liu, C., Jiang, Y.Q. and Mao, Y.K. (2013), "Substructure based structural damage detection with limited input and output measurements", *Smart. Struct. Syst*, **12**(6): 619-640.
Lei, Y., Jiang, Y. and Xu, Z. (2012), "Structural damage detection with limited input and output measurement signals", *Mech. Syst. Signal. Pr.*, **25**, 229-243**.**
Li, H.N., Yi, T.H., Gu, M. and Huo L.S. (2009), "Evaluation of earthquake-induced structural damages by wavelet transform", *Prog. Nat. Sci*, **19**(4), 461-470.
Li, J. and Law, S.S. (2012), "Substructural damage detection with incomplete information of the structure", *J. Appl. Mech. - ASME*, **79**(4), 041003.
Li, J., Law, S.S. and Ding, Y. (2012), "Substructure damage identification based on response reconstruction in frequency domain and model updating", *Eng. Struct*, **41**, 270-284.
Li, J., Law, S.S. and Hao, H. (2013), "Improved damage identification in bridge structures subject to moving loads: Numerical and experimental studies", *Int. J. Mech. Sci*, **74**, 99-111.
Li, X.Y. and Law, S.S. (2010), "Adaptive Tikhonov regularization for damage detection based on nonlinear model updating", *Mech. Syst. Signal. Pr.*, **24**(6), 1646-1064.
Lu, Z.R., Huang, M. and Liu, J.K. (2011), "State-space formulation for simultaneous identification of both damage and input force from response sensitivity", *Smart. Struct. Syst*, **8**(2), 157-172.
Lu, Z.R. and Law, S.S. (2007), "Features of dynamic response sensitivity and its application in damage detection", *J. Sound. Vib.*, **303**(1-2), 305-329.
Morton, K.W. and Mayers, D.F. (2005), *Numerical solution of partial differential equations, An Introduction*, (2nd Ed.), Cambridge University Press, UK.
Perry, M. and Koh, C.G. (2008), "Output-only structural identification in time domain: Numerical and experimental studies", *Earthq. Eng. Struct. D.*, **37**(4), 517-533.
Verboven, P., Guillanume, P., Cauberghe, S., Vanlanduit, S. and Parloo, E. (2004), "Modal parameter estimation from input-output Fourier data using frequency-domain maximum likelihood identification", *J. Sound. Vib.*, **276**(3-5), 957-979.
Wang, D. and Haldar, A. (1997), "System identification with limited observations and without input", *J. Eng. Mech. - ASCE*, **123**(5), 504-511.
Xu, B., He, J., Rovekamp, R. and Dyke, S.J. (2012), "Structural parameters and dynamic loading identification from incomplete measurements: Approach and validation", *Mech. Syst. Signal. Pr.*, **28**, 244-257.
Yan, W.J. and Ren, W.X. (2012), "Operational modal parameter identification from power spectrum density transmissibility", *Comput. - Aided Civil Infrastruct. Eng.*, **27**(3), 202-217.
Yan, Y.J., Cheng, L., Wu, Z.Y. and Yam, L.H. (2007), "Development in vibration-based structural damage detection technique", *Mech. Syst. Signal. Pr.*, **21**(5), 2198-2211.
Yang, J.N., Pan, S. and Lin, S. (2007), "Least-squares estimation with unknown excitations for damage identification of structures", *J. Eng. Mech. - ASCE*, **133**(1), 12-21.
Yi, T.H., Li, H.N. and Sun, H.M. (2013), "Multi-stage structural damage diagnosis method based on "energy-damage" theory", *Smart. Struct. Syst.*, **12**(3-4), 345-361.
Yi, T.H., Li, H.N. and Zhao, X.Y. (2012), "Noise smoothing for structural vibration test signals using an improved wavelet thresholding technique", *Sensors*, **12**(8), 11205-11220.
Zhu, H.P. and Xu, Y.L. (2005), "Damage detection of mono-coupled periodic structures based on sensitivity analysis of modal parameters", *J. Sound. Vib.*, **285**(1-2), 365-390.
Zivanovic, S., Pavic, A. and Reynolds, P. (2007), "Finite element modeling and updating of a lively

footbridge: The complete process”, *J. Sound. Vib.*, **301**(1-2), 126-145.